




Photometry of exoplanetary transits at Osservatorio Polifunzionale del Chianti

L. Naponiello¹  · L. Betti¹ · A. Biagini¹ · M. Focardi² · E. Papini¹ · R. Stanga³ · D. Trisciani³ · M. Agostini^{1,3} · V. Noce^{1,3} · L. Fini³ · E. Pace^{1,3}

Received: 26 September 2019 / Accepted: 16 July 2020 / Published online: 31 August 2020
© The Author(s) 2020

Abstract

In this paper we report the observations of HD189733b, Kepler-41b, Kepler-42b, GJ 436b, WASP-77ab, HAT-P-32b and EPIC 211818569 as measured at the Osservatorio Polifunzionale del Chianti, a new astro-nomical site in Italy. Commissioning observing runs have been done in order to test capabilities, systematics and limits of the system and to improve its accuracy. For this purpose, a software algorithm has been developed to estimate the differential photometric error of any transit observation, so that the integration time can be chosen to reach optimal signal-to-noise ratios, and to obtain a picture of what kind of transits this setup can reveal. Currently, the system is able to reach an accuracy of about 1 mmag and so it is ready for the much needed exoplanetary transit follow-up.

Keywords Extra-solar planets · Occultations · Photometry

1 Introduction

The Osservatorio Polifunzionale del Chianti (OPC) is a new astronomical site managed by the University of Florence, whose name takes origin from the different observatories that are hosted in the building. Beside the Astronomical Observatory, Geo-seismic, Meteorological and Environmental Observatories fully operate in a fruitful synergic collaboration among themselves. The observatory hosts a 80 cm aperture telescope inside a 7-m diameter dome, amid several smaller aperture class instruments, and it is located on top of one of the highest hills of the Chianti area (43° 31' 24" N - 11° 14' 44" E, 450 m above sea level), among the darkest places in Italy. All the observations documented in this paper have been done using the main telescope, which has a focal ratio of F/8 and is supported by a German equatorial mount, while its optical design is based on a Ritchey-Chretien con guration (see Fig. 1). The focal plane can host

✉ L. Naponiello
luca.naponiello@unifi.it

alternatively two CCD cameras from Moravian Instruments (G2–1600 and the new G4–9000, which has not been used for this paper) with lter wheels, both managed by means of MaxIm DL control SW from Cyanogen, and a focuser/rotator by MoonLite.

Presently, the main research activity at OPC concerns the detection of transiting exoplanets, and here we report our observations of HD189733b (Bouchy et al. 2005), Kepler-41b [1], Kepler-42b [2], GJ 436b [3], WASP-77ab [4], HAT-P-32b [5] and EPIC 211818569 [6], which are well known exoplanets that have been chosen to test the OPC setup for their availability in the needed time frame and the different signal-to-noise (S/N) ratio of their transits.

The OPC research staff is involved in national and international collaborations, like GAPS (Global Architecture of Planetary Systems) [7], which exploits several telescopes and facilities in Italy (Asiago, Osservatorio Autonomo della Valle d'Aosta) and Canary Islands (HARPS-North and GIANO instruments as well as their improved combined version installed at the Italian Telescopio Nazionale Galileo) for exoplanetary characterization, and the TESS (Transiting Exoplanet Survey Satellite) SG1 (Sub-group 1) follow-up [8] as well as the KFUN (KELT Follow-up Network) [9] for the observation of exoplanet candidates. OPC researchers perform their activity in the framework of collaborations with the INAF-Osservatorio astrofisico di Torino and the Osservatorio Autonomo della Val d'Aosta. The authors also aims at the observation of the optical/visible counterpart of gamma ray bursts afterglows, young stellar objects, supernovae and Gravitational Waves (GW) Target of Opportunity (ToO) follow-up.

The transit method is the most successful for detecting new exoplanets and it is based on the measurement of stellar flux variations when the planet transits in front of its star, therefore large planets orbiting around small stars with a short period are easier to find since they can be detected multiple times in a relative short period of time. The only detectable planetary systems with this method, however, are those that have orbital planes almost aligned to our line of sight, and their transit depth is proportional to the ratio $(R_p / R)^2$, where R_p and R are respectively the radius of the planet and the star. Some more parameters can be estimated from transit observations, like the inclination of the orbit in respect to our line of sight, its major axis, and in particular cases even the coefficients that characterize the limb darkening effect [10]. Radial velocity measurements, along with the Rossiter-McLaughlin effect [11] and transit spectroscopy [12], are required to further evaluate the properties of the planetary systems (Jason T. [13]).

Usually large-aperture, ground-based telescopes are employed to characterize known exoplanets for instance by analyzing their atmosphere with transit spectroscopy, and do not have the time to follow-up the numerous new exoplanet candidates captured

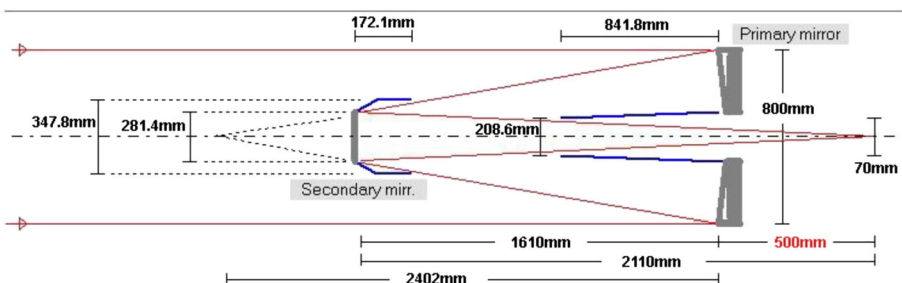


Fig. 1 Optical design of the 80 cm aperture telescope at OPC, property of Università di Torino

by transiting wide-field surveys such as TESS and other coming satellites like PLATO [14]. These surveys are built to look at a large number of stars at once, so their pixel scales are larger than the sub-arcsec pixels that ground-based telescopes employ. This means that many candidates flagged by said surveys could be false positives due to unresolved eclipsing binaries (EB) blended with one or more stars, and to other types of contamination. In order to identify real exoplanets, such systems have to be observed from the ground with smaller pixel scales and extensive time (as long period exoplanets would only show up once or twice in the time frame of a wide-field survey satellite, and thus can hardly be confirmed). Moreover, transit ephemeris often have large error bars which scale with passing time, so observing more transits from the ground is of high importance in order to reduce said errors for future observations. The ExoClock project,¹ for example, has recently born to gather light curves that will be used by the ARIEL space mission [15] for the improvement of transit timing accuracies, and the OPC is one of the contributing observatories. According to Zellem et al. [16] precise mid-transit time predictions would enable space missions to act more efficiently, so much that transit maintenance with a network of sixteen 15 cm aperture telescope could save up to 100 days of ARIEL observing time during its nominal mission lifetime of 3.5 years.

2 Error estimation

In order to be able to detect an exoplanetary transit, many images of the target star have to be acquired and its flux has to be normalized to the constant flux of some reference stars in the same field for each image (see Fig. 2), to correct for luminosity variations due to larger effects like light pollution, small changes of focus, airmass, Moon distance and so on. This technique is called differential photometry and it allows for the observation of relatively low depth transits even within the Earth’s atmosphere.

Each stellar flux count has approximately the following S/N ratio, expressed in analog to digital units or ADU (for a detailed description of each source of noise see Merline et al. [17]):

$$\frac{S}{N} \approx \frac{I^*}{\sqrt{I^* + \eta_{pix} \left(1 + \frac{\eta_{pix}}{\eta_B} \right) \left(I_S + \frac{I_D}{G} + \frac{N_r}{G} \right)}}, \tag{1}$$

where η_{pix} and η_B are respectively the pixels of the aperture area and the outer annulus surrounding each star inside which the sky background luminosity is estimated. I , I_S , and I_D are respectively the ux of the star (ADU), the ux of the background (ADU/pixel) and the dark signal (electrons/pixel). Finally, G represents the gain of the CCD (electron/ADU, 1.5 for the G2 camera) and N_r the readout noise which is a camera-speci c (electrons/pixel per read, 15 for the G2). Another source of noise is scintillation [18], which can be added in quadrature to find the overall error. It can be estimated using Dravin’s (or Young’s) equation:

¹ For more information go to the website: <https://www.exoclock.space/>

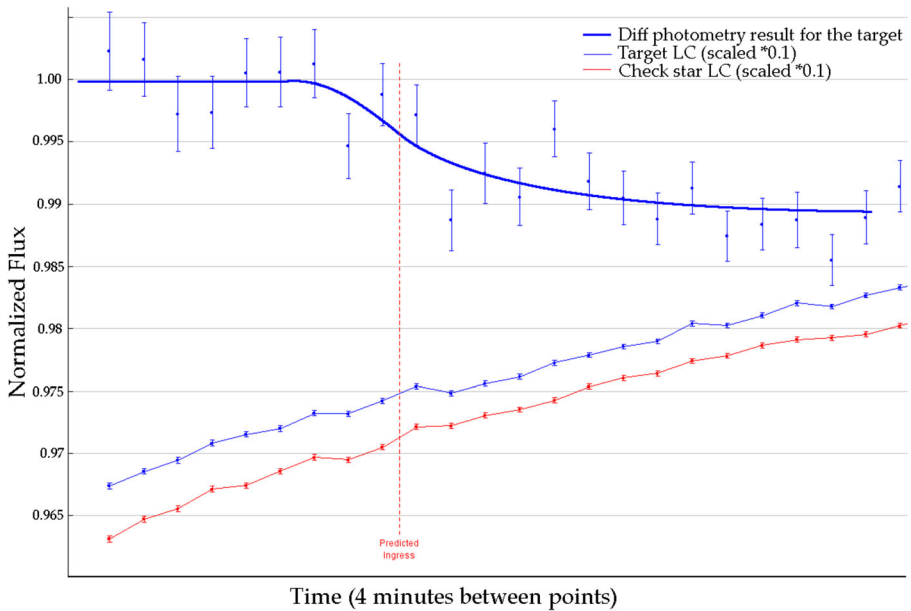


Fig. 2 Example of differential photometry for the observation of Kepler-41b. The light curve (LC) on top is obtained by normalizing the blue curve below using the LC of the reference star in red

$$\sigma_{scint} = \frac{0.003D^{-2/3}X^{7/4}e^{-h/H}(2t_{exp})^{-1/2}}{3} \tag{2}$$

where D is the effective aperture of the telescope in meters, X is the airmass (which is a function of the star zenith distance), t_{exp} is the integration time, $H = 8000$ m is the atmosphere scale height, and h the height of the location site compared to sea level. The number coefficient (0.003) is slightly dependent on humidity, while the power of X oscillates between $6/4$ and $8/4$ according to the wind direction. Note that scintillation noise is likely to be underestimated up to a 1.5 factor especially for very bright sources [19], though for the purpose of estimating the noise to find good integration times, which we are about to discuss, this level of precision is not needed because again scintillation noise becomes important mainly for low magnitude stars (most of the candidates orbit around faint and/or distant stars) and the integration times in general are not much affected. Finally, each error is then propagated to find the error for the normalized flux of the target star:

$$\sigma_{flux} = \frac{F_T}{F_E} \sqrt{\sigma_T^2 + \sigma_E^2} \tag{3}$$

where σ_T (F_T) and σ_E (F_E) are respectively the relative errors (flux counts) calculated for the target star and the ensemble of reference stars. Knowing all the instrumental and physical parameters of the observation, namely the magnitude of the target and the reference stars, CCD gain and readout noise, target field altitude (i.e. airmass),

telescope diameter, seeing and average background luminosity; an evaluation of the statistical error can be done for different integration times.² At this point the minimum of the ratio of error over time provides the integration time required to achieve the best S/N ratio for the observation.

Note that a longer integration time often requires images to be taken out of focus [20] to avoid saturating any pixel or exceeding their linearity limit. In this case, increasing the integration time reduces all relative noises but the Poisson background contribution, because defocussing increases the size of star images by spreading their light on more pixels (enlarging the FWHM), thus reducing the available space that is used to estimate the sky background between the stars. Moreover, the integration time should be kept as short as possible for a precise evaluation of the transit parameters, which especially require a decent sampling of the high variability events, e.g. ingress and egress.

3 Algorithm

Taking inspiration from Southworth et al. [21] and using the above formulas, the authors have written an algorithm that estimates the best observational parameters in order to achieve the highest S/N for a certain filter bandwidth. Given a set of general instrument-based constants (e.g. G , N_r , D and so on) the user simply has to insert some specific star parameters like the average airmass of the star field during a particular night and the star fluxes in ADU, on a case-by-case basis. Particularly critical is the background noise parameter (named $C(B)$ in figure 4, as ADU/pixel/s) and its evaluation has to be done right before the observation because it depends on the field, the filter used and the average sky luminosity of the night due to the Moon presence for example. In the end, the user receives a suggested integration time³ and plots like Fig. 3 and Fig. 4, which will now be explained. In the observation of HD189733b (Figure 6) the background luminosity was quite high and as a consequence the suggested exposure time was only around 30 s.

The main test for this algorithm was to apply it to HD189733b, a planet providing a transit depth around 2.5% (Bouchy et al. 2005) which is easily accessible for the performance of the OPC optical system. Figure 3 shows the predicted errors at different integration times, highlighting the fact that the seeing is the major source of error for the differential photometry applied to a star of visible magnitude 7.6 (HD 189733) at OPC. The Poisson noise for the background though is the limiting factor for the integration time (blue line in figure 3), as expected. The final uncertainty for the normalized target flux is found by combining all the source of errors using Eqs. 1 and 3, and then the relative noise per unit time is plotted in function of the integration

² One important observation overhead is the download time, here defined as the overall time that passes between the end of one integration and the beginning of the next one, as it is basically a waste of transit time and its total sum gets longer with shorter exposures (for the G2–1600 camera, the download time is around 3.5 s).

³ Note that the algorithm has to know the shape of the PSF response of the imaging system, since it can't suggest an integration time that would saturate pixels or reduce too much the space available to evaluate background luminosity in a crowded field.

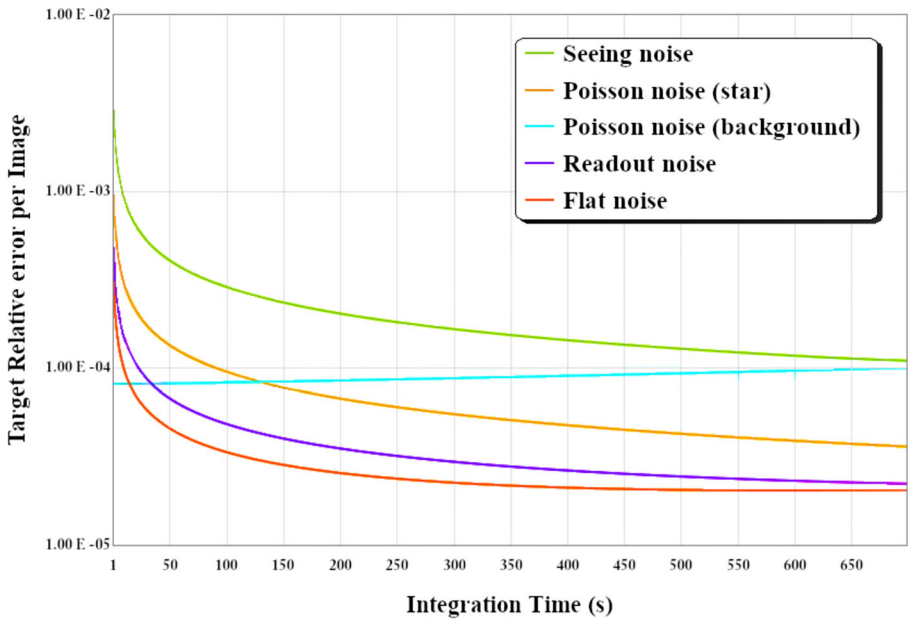


Fig. 3 Evaluation of the main noise sources as estimated by using the algorithm for the observation of HD189733b at OPC, by far the brightest star of our sample, at different integration times (in seconds)

time (as seen in Fig. 4). The minimum valley of this curve represents the integration time values which result in the highest S/N ratio.

Di different combinations of reference stars in the field were used but the results always had an estimated error very close to the one found minimizing the X^2 of each

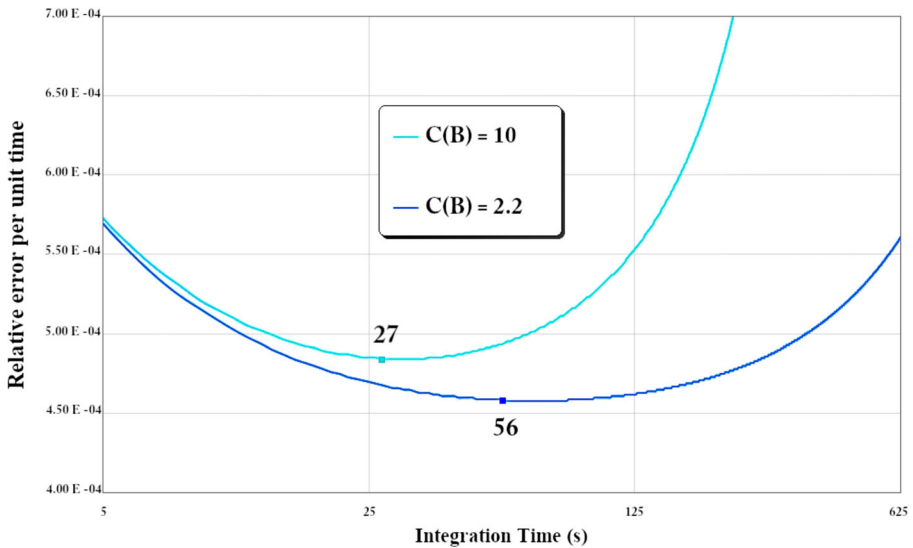


Fig. 4 Final uncertainty per unit time for the target star HD189733, in case of two different background luminosity coefficients. Note that the higher the background luminosity is, the shorter the integration time must be, since the pixels saturate faster

σ_P	σ_C	$\frac{\sigma_P}{\sigma_C}$	$\frac{F_T}{F_E}$	C2	C3	C4	C5	C6	C7	C8
				10.7	9.4	9.1	11.1	11.5	11	10.8
1.7	1.7	≈ 1	1.58	x	x	x	x	x	x	x
1.8	1.7	≈ 1	1.65	x	x	x	x		x	x
1.8	1.8	≈ 1	1.72	x	x	x	x	x	x	
1.8	1.8	≈ 1	2.1	x	x	x				
1.8	1.8	≈ 1	2.23	x		x	x	x	x	x
1.9	1.9	≈ 1	2.54			x	x	x	x	x
2.2	2.3	≈ 1	5.45		x					
2.1	2.3	≈ 0.9	8.33					x	x	x
2.5	2.4	≈ 1	17.9	x						
3.4	3.8	≈ 0.9	38.7					x		

Fig. 5 Comparison of predicted (σ_P) versus real (σ_C) noise for the observation of HD189733b with different combinations of reference stars (C2, C3 and so on, with their respective visible magnitude below), while F_T/F_E is the ratio between the target star flux and the sum of the flux of the reference stars

model t (up to 10%, see Figure 5), and the result of the best combination of check stars is shown in Fig. 6, where every point represents a total integration time of 210 s (as obtained from binning single exposures of 30 s) for viewing purpose only. The data has been elaborated with the photometric software AstroImageJ [22] and then the parameter errors have been derived by means of a Markov Chain Monte Carlo (MCMC) analysis. The radius found is 1.18 ± 0.07 times the radius of Jupiter, in accordance with various sources (De Kok et al. [23]).

Using this tool, it is possible to make a rough estimation of the observational limit for the OPC optical system by studying how the expected error varies with the stellar magnitude and by comparing it to the transit depths. Figure 7 shows the transit depth of

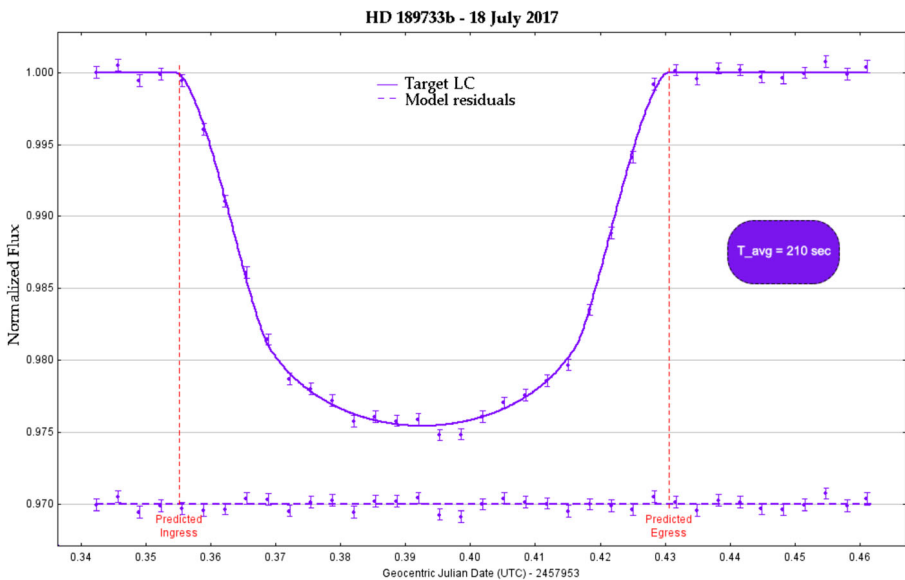


Fig. 6 HD189733b (apparent star magnitude $V = 7.6$) transiting light curve, as obtained the 18th of July 2017 at OPC

known transiting exoplanets from the NASA catalogue (with accurate depths, as of February 2018) versus the optical magnitude of their star; the blue line represents the transit depth values comparable to the estimated error on the normalized stellar flux, while the green line represents transit depths 5 times larger than the error of the normalized stellar flux (note that the error also changes according to the sky background luminosity, availability of reference stars and, above all, the stars altitude during the observation). According to Figure 7, roughly 70% of known transits could be studied at OPC, while 20% of them would be at the limit of observability (but still observable enough to check transit ephemeris). The remaining 10% lies beyond the sensitivity of the instrument.

4 Results and conclusions

Seven exotransits of different star magnitudes and depths have been observed at OPC in order to confirm the predicted observational limit of the setup (Figs. 6, 8, 9, 10, 11, 12 and 13), and three of them have been analyzed with the MCMC method, using the TAP software (Transit Analysis Package) for IDL [24], as it has been detailed in Table 1. HAT-P-32b is a Jupiter-size bloated planet [25] that orbits a G/F type star (visible magnitude = 11.2), 950 light years away from Earth, with a major semiaxis of 0.034 AU and an orbital period of just 2.15 days (suggested and chosen integration time for this observation: 120 s). WASP-77ab is also an inflated Jupiter transiting every 1.36 days in front of its star, which has a visible apparent magnitude of 11.3, with a major semiaxis of 0.024 AU [4]. For this observation the chosen integration time was instead 40 s. Both these transits are easily detectable as expected.

Gliese 436 is a red dwarf only 30 ly away, and its apparent visible magnitude is below the value of 11. The only known planet has an orbital period of 2.6 days and is 0.3 AU distant from the star [3]. This observation was unfortunately affected by thin clouds and as a result the noise was higher than expected, but the transit dip was still easily visible (with an integration time of 20 s due to high background noise; in the plot the points have been binned 9x). EPIC 211818569 or K2-121 is at least a 2-planet system [26], orbiting a 13.3 apparent visible magnitude star. The planet b that we

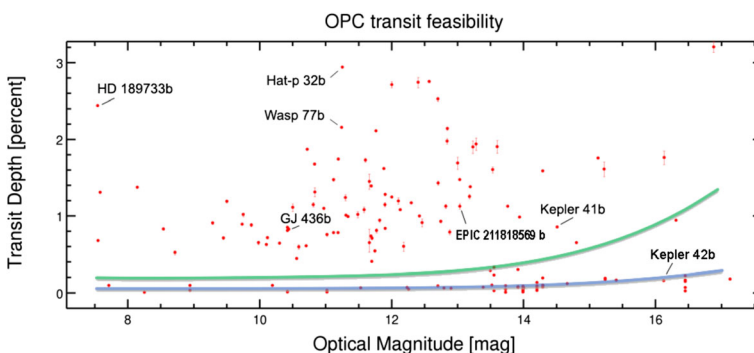


Fig. 7 Red dots are stars from the NASA archive with confirmed transits of known depth (as of February 2018). The indicated exoplanets are those presented in this paper

HAT-P-32 b

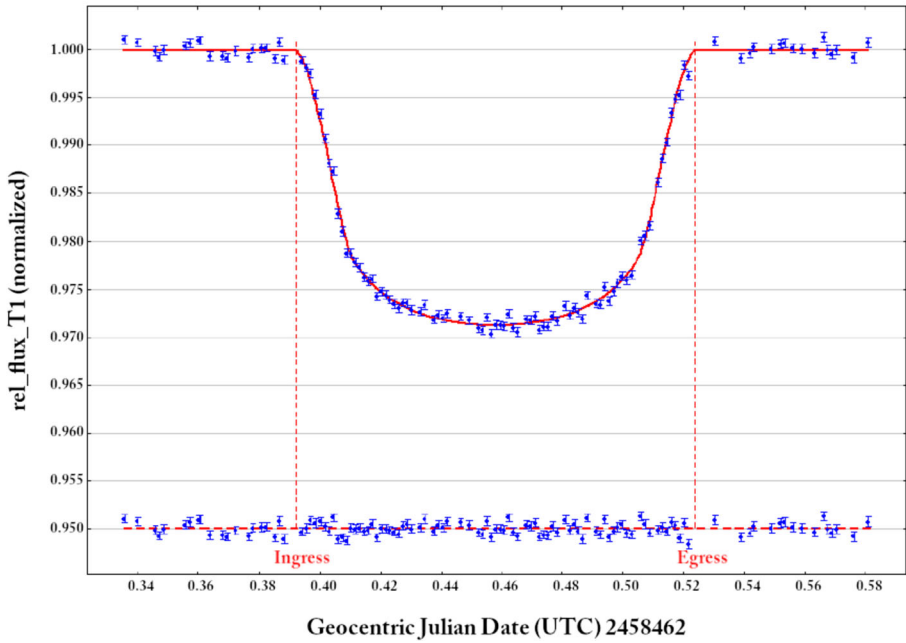


Fig. 8 Light curve of HAT-P-32b (apparent star magnitude $V = 11.2$), observed on December 9th 2018

WASP-77 Ab

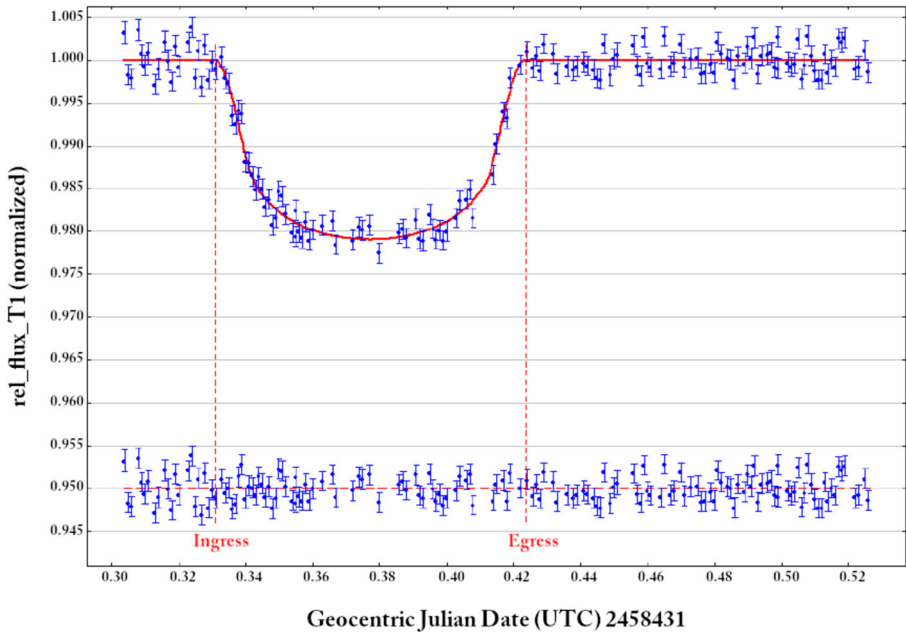


Fig. 9 Light curve of WASP-77ab (apparent star magnitude $V = 11.3$), taken on November 8th 2018

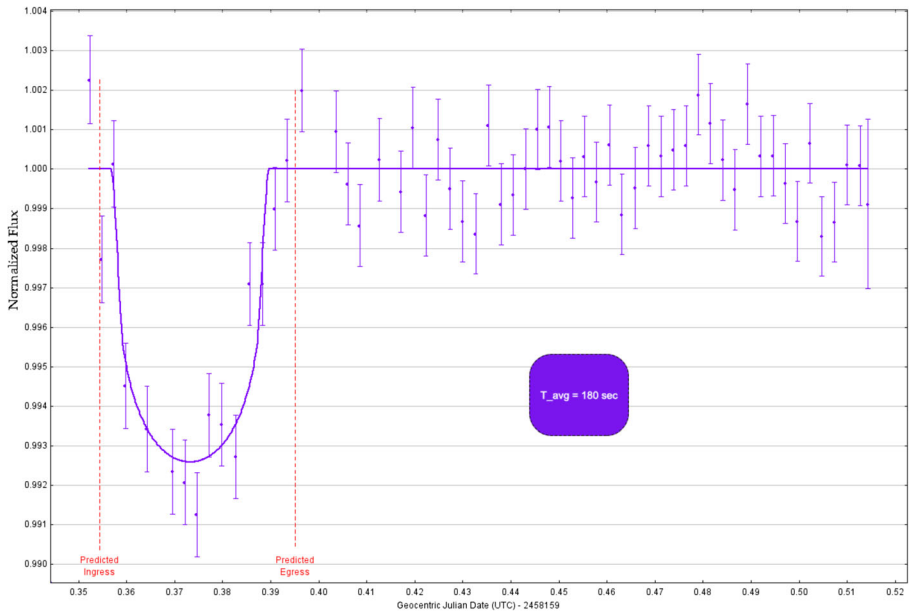


Fig. 10 GJ 436b (apparent star magnitude $V = 10.7$) light curve as observed on February 9th, 2018. Each point represents 180 s of exposure and the S/N ratio is lower than expected due to weather issues

observed is a small Jupiter which was again easily detected by our setup with an integration time of 120 s as suggested by our algorithm.

Kepler-41 is a yellow dwarf similar to the Sun, 2380 light years away and with a visible apparent magnitude of 14.5 [1]. Its planet, Kepler-41b, seems to be a mild

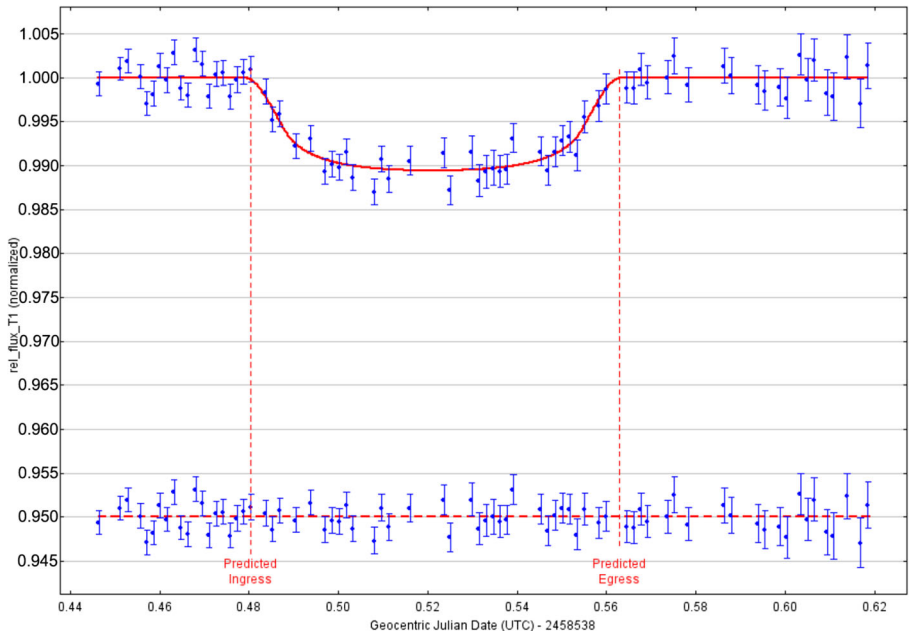


Fig. 11 Light curve of EPIC 211818569 (apparent star magnitude $V = 13.3$), observed on February 23rd 2019

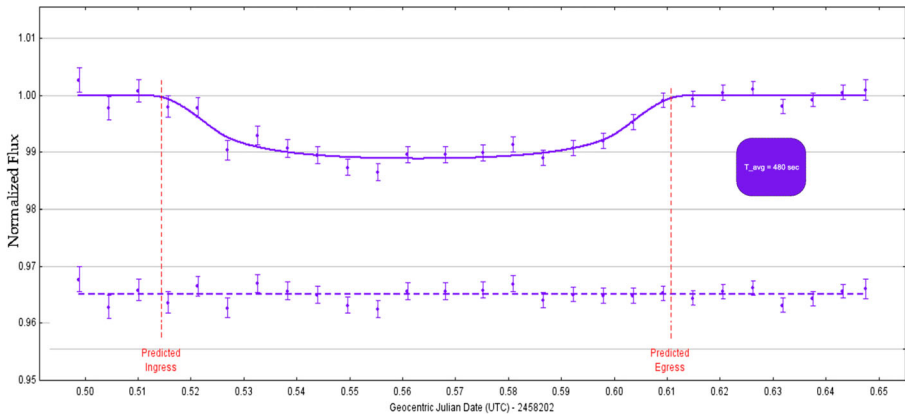


Fig. 12 Light curve of Kepler-41b (apparent star magnitude $V = 14.5$) as observed on March 25th, 2018, with a low altitude field of 30° . Each point represents 480 s of exposure and the S/N ratio is getting close to the size of the transit depth as expected by the transit feasibility study

Jupiter with a orbital radius of 0.03 AU, in a 1.86 day period. The suggested integration time was 240 s and in Figure 12 the points have been binned to be 480 s long. As predicted in Fig. 7 we are reaching the observational limit of the OPC setup. Kepler-42 is a red dwarf just a bit larger than Jupiter, 126 light years away and with a visible apparent magnitude of 16.15, the dimmer star of our sample. This system has 4 known planets, and Kepler-42b in particular is Earth-sized, has a major semiaxis of only 0.012 AU and an orbital period of 1.2 days [2]. This transit is past the expected observational limit, and infact each point uncertainty is comparable to the transit depth.

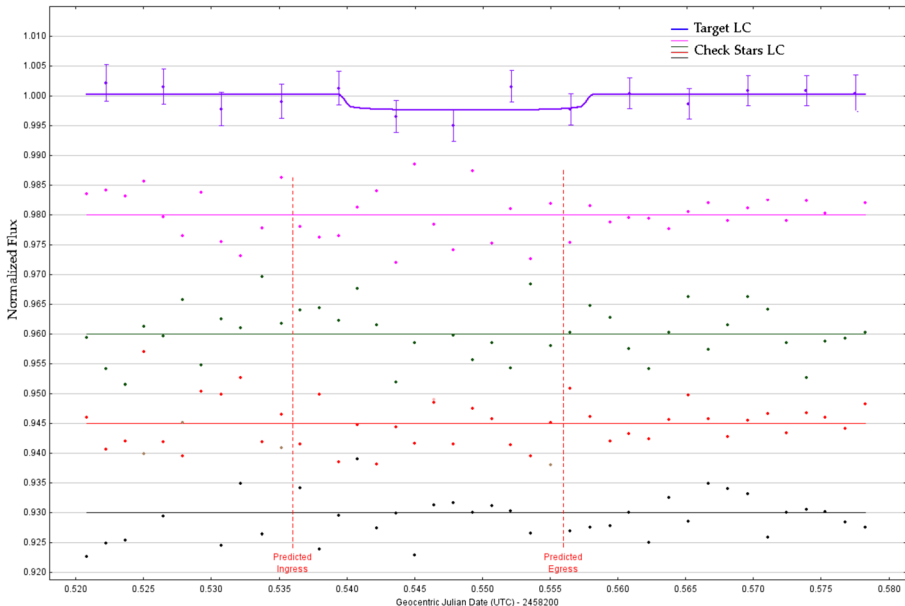


Fig. 13 Kepler 42-b tentative light curve for a 16.15 apparent visible magnitude star, from the 23rd of March 2018. The transit cannot be appreciated and no information can be extracted from this observation

Table 1 Comparison between the transit parameters with their uncertainties found by means of Markov Chain Monte Carlo analysis, and the respective values found on their original papers (propagated to the epoch of the observations, for the Mid Transit). We don't find any significant deviation.

WASP-77Ab		
Parameters	MCMC	Maxted et al. (2012)
Inclination (degrees)	88:9±0:2	88:92±0:10
a/R_*	6:04±0:03	6:056±0:009
$(R_p=R_*)^2$	0:1503 ^{+0.0013} -0.0014	0:1510±0:0004
Mid Transit (BJD_{TDB})	2458462:4624±0:0003	2458462:4620±0:00032
HAT-P-32b		
Parameters	MCMC	Seelinger et al. (2014)
Inclination (degrees)	88:9±0:2	88:92±0:10
a/R_*	6:04±0:03	6:056±0:009
$(R_p=R_*)^2$	0:1503 ^{+0.0013} -0.0014	0:1510±0:0004
Mid Transit (BJD_{TDB})	2458462:4624±0:0003	2458462:4620±0:00032
Parameters	MCMC	Mayo et al. (2018)
EPIC 211818569		
Inclination (degrees)	89.4 ^{+0.02} -0.03	89:03 ^{+0.57} -0.54
a/R_*	19:2 ^{+0.8} -0.4	20:1 ^{+0.9} -1.3
$(R_p=R_*)^2$	0:1037 ^{+0.0017} -0.0023	0:1021 ^{+0.0040} -0.0023
Mid Transit (BJD_{TDB})	2458538:5259 ^{+0.0027} -0.0031	2458538:5296±0:0039

No information at all can be extracted from the tentative light curve shown in Figure 13 (integration time is 120 s, binned 3x).

The calculated parameters we summarized in Table 1 are in good agreement with the literature, in particular the transit mid times have smaller error bars compared to the expected mid times, which uncertainties we have derived by propagating the original estimation errors.⁴ So, while it is true that the transit method is mostly used in space to find new exoplanetary candidates, having follow up transit observations is also very important both for the confirmation of such candidates and in particular for the ephemeris maintenance. The predictive algorithm proved to be a useful tool to understand the limits of the OPC setup and to optimize ground observations of transiting exoplanets, so that even small-medium size telescopes as the OPC 80 cm can be effective in the follow up observations, by being able to reach sub millimag average errors for the flux of stars below magnitude 11, and millimag average errors for stars between magnitude 11 and 14.

⁴ There's no need to update the ephemeris since we don't find significant deviations between our fit and the predicted times, but this proves the potential of transit maintenance for small-sized telescopes contribution.

Acknowledgments We thank the Rotary Club (San Casciano - Chianti) for funding two study grants, to LB and AB, and Karen Collins for some fruitful conversations at the beginning of this work. We also thank the anonymous referee for providing many useful suggestions.

Funding Information Open access funding provided by Università degli Studi di Firenze within the CRUI-CARE Agreement.

Open Access This article is licensed under a Creative Commons Attribution 4.0 International License, which permits use, sharing, adaptation, distribution and reproduction in any medium or format, as long as you give appropriate credit to the original author(s) and the source, provide a link to the Creative Commons licence, and indicate if changes were made. The images or other third party material in this article are included in the article's Creative Commons licence, unless indicated otherwise in a credit line to the material. If material is not included in the article's Creative Commons licence and your intended use is not permitted by statutory regulation or exceeds the permitted use, you will need to obtain permission directly from the copyright holder. To view a copy of this licence, visit <http://creativecommons.org/licenses/by/4.0/>.

References

1. Barstow, J., et al.: Transit spectroscopy with JWST: systematics, star-spots and stitching. *Monthly Notices of the Royal Astronomical Society*. **451**(2), 1306–1306 (2015). <https://doi.org/10.1093/mnras/stv1041>
2. Bouchy, F., et al.: ELODIE metallicity-biased search for transiting Hot Jupiters II. A very hot Jupiter transiting the bright K star HD 189733. *Astronomy and Astrophysics*. **444**(1), L15–L19 (2005). <https://doi.org/10.1051/0004-6361:200500201>
3. Collins, K.A.: AstroimageJ: Image processing and photometric extraction for ultra-precise astronomical light curves. *The Astronomical Journal*. **153**(2), (2017)
4. Collins, K.A.: TESS Follow-up Observing Program (TFOP) Working Group: A Mission-led Eort to Coordinate Community Resources to Conrm TESS Planets. *American Astronomical Society, AAS Meeting 231*, id. 439.08. (2018)
5. Collins, K.A.: The KELT Follow-Up Network and Transit False Positive Catalog: Pre-vetted False Positives for TESS. *The Astronomical Journal*. **156**, 5 (2018)
6. Kok, D., et al.: Detection of carbon monoxide in the high-resolution day-side spectrum of the exoplanet HD 189733b. *Astronomy and Astrophysics*. **554**, A82 (2013). <https://doi.org/10.1051/0004-6361/201321381>
7. Gazak, J.Z., et al.: Transit Analysis Package (TAP and autoKep): IDL Graphical User Interfaces for Extrasolar Planet Transit Photometry. *Advances in Astronomy*. (2012, Article ID 697967, 8 pages). <https://doi.org/10.1155/2012/697967>
8. Hartman, J.D., et al.: HAT-P-32b and HAT-P-33b: Two Highly Inated Hot Jupiters Transiting High-Jitter Stars. *The Astrophysical Journal*. **742**, 1 (2011)
9. Zellem, R., et al.: Utilizing Small Telescopes Operated by Citizen Scientists for Transiting Exoplanet Follow-up. *Bulletin of the American Astronomical Society*. **52**(1), (2020)
10. Magrin, D., et al.: PLATO: the ESA mission for exo-planets discovery. *Proceedings of the SPIE*. **10698**, (2018) 106984X-10
11. Maxted, P.F.L., et al.: WASP-77 Ab: A transiting hot Jupiter planet in a wide binary system. *Publications of the Astronomical Society of the Pacic*. **125**(923), (2012)
12. Mancini, L., et al.: The GAPS Programme with HARPS-N at TNG XVII: Measurement of the Rossiter-McLaughlin effect of the transiting planetary systems HAT-P-3, HAT-P-12, HAT-P-22, WASP-39 and WASP-60m. (2018). <https://doi.org/10.1051/0004-6361/201732234>
13. Mayo, A.W., et al.: VizieR Online Data Catalog: Planets orbiting bright stars in K2 campaigns 0-10. *The Astrophysical Journal*. **155**, 136 (2018)
14. Merline, W.J., Howell, W.J., et al.: A realistic model for point-sources imaged on array detectors: the model and initial results. *S.B. Exp Astron*. **6**, 163 (1995). <https://doi.org/10.1007/BF00421131>
15. Muirhead, P., et al.: haracterizing the Cool KOIs III. KOI-961: A Small Star with Large Proper Motion and Three Small Planets. *The Astrophysical Journal*. **747**(2), (2012). <https://doi.org/10.1088/0004-637X/747/2/144>

16. Ohta, Y., et al.: The Rossiter-McLaughlin Effect and Analytic Radial Velocity Curves for Transiting Extrasolar Planetary Systems. *The Astrophysical Journal*. **622**(2), (2005)
17. Osborn, J., et al.: Atmospheric Scintillation in Astronomical Photometry. *Monthly Notices of the Royal Astronomical Society*. **452**(2), (2015). <https://doi.org/10.1093/mnras/stv1400>
18. Pope, B., et al.: Atmospheric Scintillation in Astronomical Photometry. *Monthly Notices of the Royal Astronomical Society*. **461**(4), (2006). <https://doi.org/10.1093/mnras/stw1373>
19. Ribas, I., et al.: A 5 Earth mass Super-Earth Orbiting GJ 436?: The Power of Near-Grazing Transits. *The Astrophysical Journal Letters*. (2008). <https://doi.org/10.1086/587961>
20. Santerne, A., et al.: SOPHIE velocimetry of Kepler transit candidates IV. KOI-196b: a non-inflated hot Jupiter with a high albedo. *Astronomy and Astrophysics*. 536.A70 (2011). <https://doi.org/10.1051/0004-6361/201117807>
21. Southworth, J., Hinse, T.C., et al.: High-precision photometry by telescope defocussing. I. The transiting planetary system WASP-5. *Monthly Notices of the Royal Astronomical Society*. **396**(2), 1023–1031 (2009)
22. Seager, S., et al.: On the Unique Solution of Planet and Star Parameters from an Extrasolar Planet Transit Light Curve. *The Astrophysical Journal*. **585**(2), (2002)
23. Seelinger, M., et al.: Transit Timing Analysis in the HAT-P-32 system. *Monthly Notices of the Royal Astronomical Society*. **441**(1), (2014)
24. Tinetti, G., et al.: The science of ARIEL. Proc. SPIE 9904, Space Telescopes and Instrumentation 2016: Optical, Infrared, and Millimeter Wave. 99041X (2016). <https://doi.org/10.1117/12.2232370>
25. Wright, J.T.: Radial Velocities as an Exoplanet Discovery Method. arXiv. 1707.07983 (2017)
26. Young, A.T., et al.: Photometric error analysis. VI. Confirmation of Reiger's theory of scintillation. *The Astronomical Journal*. **72**, 747 (1967). <https://doi.org/10.1086/110303>

Publisher's note Springer Nature remains neutral with regard to jurisdictional claims in published maps and institutional affiliations.

Affiliations

L. Naponiello¹ · L. Betti¹ · A. Biagini¹ · M. Focardi² · E. Papini¹ · R. Stanga³ · D. Trisciani³ · M. Agostini^{1,3} · V. Noce^{1,3} · L. Fini³ · E. Pace^{1,3}

L. Betti
l.betti@osservatoriochianti.it

A. Biagini
alfredo.biagini93@live.it

M. Focardi
m.focardi@osservatoriochianti.it

E. Papini
papini@arcetri.inaf.it

R. Stanga
ruggero.stanga@gmail.com

D. Trisciani
damiano@tnx.it

M. Agostini
m.agostini@osservatoriochianti.it

V. Noce
vladimiro.noce@inaf.it

L. Fini
luca.fini@gmail.com

E. Pace
e.pace@osservatoriochianti.it

- ¹ Dipartimento di Fisica e Astronomia, Università degli Studi di Firenze, via G. Sansone 1, I-50019 Sesto Fiorentino, Italy
- ² INAF, Osservatorio Astrofisico di Arcetri, Largo E. Fermi 5, 50125 Florence, Italy
- ³ Osservatorio Polifunzionale del Chianti, Barberino Val d'Elsa, Florence, Italy